Modelling of size and shape of damage zone in quasi-brittle notched specimens – analytical approach based on fracture-mechanical evaluation of loading curves

J. Klon, V. Veselý
Brno University of Technology, Faculty of Civil Engineering, Institute of Structural Mechanics, Veveří 331/95, 602 00 Brno, Czech Republic
klon.j@fce.vutbr.cz
vesely.v1@fce.vutbr.cz, http:/orcid.org/0000-0002-7723-971X

ABSTRACT. An analysis focused on capturing the phenomenon of quasi-brittle fracture is presented. Selected parameters relevant for quasi-brittle fracture are evaluated and an assessment of their dependence on the size and shape of the test specimen is studied. Determination of these fracture characteristics is based on the records of the fracture tests on notched specimens, particularly from recorded loading diagrams. A method of separation of the energy amounts released for the propagation of the (effective) crack and that dissipated within the volume of a large nonlinear zone at the crack tip – the fracture process zone – is introduced and tested on selected data from experimental campaigns published in the literature. The work is accompanied with own conducted numerical simulations using commercial finite element code with implemented cohesive crack model. Results from three-point bending tests on specimens of different sizes and relative notch lengths are taken into account in this study. The proposed model has only two parameters whose values are constant for all specimen sizes and notch lengths.

KEYWORDS. Quasi-brittle Fracture; Loading Curve; Work of Fracture; Resistance Curve; Effective Crack; Fracture Process Zone.

OPEN ACCESS

Citation: Klon, J., Veselý, V., Modelling of size and shape of damage zone in quasi-brittle notched specimens – analytical approach based on fracture-mechanical evaluation of loading curves, Frattura ed Integrità Strutturale, 39 (2017) 17-28.

Received: 20.07.2016
Accepted: 21.09.2016
Published: 01.01.2017

INTRODUCTION

Fracture properties of quasi-brittle materials, corresponding to commonly used fracture models relevant to this type of fracture behaviour, appear to be dependent on the test specimen size, shape and boundary conditions. This fact has been well recognized in the last five or six decades (summarized in e.g. [1–4]). The reason for that is in the existence of a large zone of nonlinearly behaving material around the tip of the propagating crack. The major part of this zone is referred to as the *fracture process zone* (FPZ), in which mechanisms of material toughening take a place. These

mechanisms cause the so-called tension softening of the material and can be particularly regarded as interpretation of the crack bending around aggregates, friction of cracks face and aggregate interlock, blinding of crack tip in pores, crack branching and others [1,3].
There were many attempts to capture/deal with the phenomena of the size/shape/boundary effect on fracture properties of quasi-brittle materials proposed with success in the last more than twenty years [5–14]; however, the applicability/validity of the suggested remedies are usually rather limited and not general.
This is true also for the standardized work-of-fracture method for determination of fracture energy of concrete [15]. The value of fracture energy determined by this method is strongly dependent on the specimen size and geometry [9,10,12] This phenomenon is caused by the change in the size and shape of the FPZ during crack propagation, from which the change of energy dissipated in this area results. This change is determined by the distance and the position of the crack tip and the FPZ in relation to free surfaces of the specimen [12]. Therefore, the existence of the FPZ begins to be taken into account recently in the context of models describing quasi-brittle fracture, which is also the aim of this study.
Thus, also own attempts to capture the abovementioned effects, in this case via an incorporation of the real size and shape of the FPZ at the crack tip to the method of evaluation of the fracture characteristics, have been introduced [16–18]. To identify the properties of FPZ, a combination of adaptation of linear elastic fracture mechanics (LEFM) (which is used to express the amount of energy released for creation of the new surface of an effective crack without considering the existence of FPZ) and cohesive-crack-based fracture models for concrete and other quasi-brittle materials [19,20] (which enable the modelling of the FPZ extent) was proposed. This method models the FPZ in detail during the whole fracture process along the specimen ligament. However, its relation to the energetic evaluation of the fracture process was suggested only schematically. Basically, it divides the energy dissipated for the fracture into the part released for propagation of the effective crack and that released in the FPZ volume corresponding to the current stage of fracture process [21]. Therefore, further analyses have been conducted [22, 23].
This present paper follows and extends on those mentioned works. It is focused on the evaluation of selected fracture parameters of concrete and particularly on the assessment of their dependence on the size and shape of the test specimen. The envelope of FPZ extents evolving during fracture and the fracture resistance are among the investigated parameters. The whole analysis regards two sets of three-point bending tests on notched beams of varying sizes and notch lengths published in [24] and [25,26].

CONCEPTUAL APPROACH

Modelling of energy dissipation during quasi-brittle fracture process through the specimen ligament

The nonlinear fracture is treated in this work via a division of the energy released for the fracture propagation into two parts. This separation is performed on the level of processing of the recorded P–d diagram, where P is the applied load and d is the load-point displacement. It is treated on the level of evaluation of the work of fracture (its infinitesimal increment),

$$\mathrm{d}W_{\mathrm{f}}(a) = \mathrm{d}W_{\mathrm{f,b}}(a) + \mathrm{d}W_{\mathrm{f,fpz}}(a) \quad [\mathrm{J}] \tag{1}$$

which represents the area under the P–d diagram. Here, $\mathrm{d}W_{\mathrm{f,b}}$ (subscript 'b' denotes 'brittle') is the energy release connected with creation of new fracture surfaces and $\mathrm{d}W_{\mathrm{f,fpz}}$ (with 'fpz' denoting 'fracture process zone') is the energy dissipated in the volume of the current FPZ.
The energy released for the creation of the new fracture surface increment can be specified by its area, i.e. $\mathrm{d}a_{\mathrm{ef}} \cdot B$, where a_{ef} is the effective crack length (marked simply as a in the further text) and B is the specimen thickness. This leads to the well-known definition of the fracture characteristics (of LEFM), the toughness,

$$G_{\mathrm{f}}(a) = \frac{1}{B}\frac{\mathrm{d}W_{\mathrm{f,b}}(a)}{\mathrm{d}a} \qquad [\mathrm{Jm}^{-2}] \tag{2}$$

The term fracture energy (instead of toughness) is used for this quantity mainly in the field of quasi-brittle cementitious composites like concrete. Accordingly, the $\mathrm{d}W_{\mathrm{f,fpz}}$ part should be specified by the FPZ volume, which leads to the expression of a quantity describing the density of the energy dissipation in the FPZ,

$$H_f(A_{fpz}) = \frac{1}{B}\frac{dW_{f,fpz}(A_{fpz})}{dA_{fpz}} \qquad [Jm^{-3}] \qquad (3)$$

The symbol A_{fpz} represents the cumulative area of the FPZ, referred to as the cumulative damage zone (CDZ) here. It means that a unification of all FPZ's extents from the beginning of the crack propagation from the initial notch to the current fracture stage. It is assumed in the approach that FPZ extent doesn't vary over the specimen thickness B. In addition, the parameter G_f is considered to be constant during the fracture propagation.
In this work, however, the model is even much more simplified. The parameter H_f is supposed to be of uniform distribution over the FPZ extent, which is definitely an unrealistic assumption. However, it is taken into account for its simplicity as an initial step towards verification/assessment of the proposed concept. Then, the real area of the current CDZ (of the volume $A_{fpz}\cdot B$) doesn't enter the procedure, since the current shape of that zone is uneasy to express. Instead, a rectangular increment of the cumulative FPZ area expressed as $\delta a\cdot t$ is considered. Here, t is the FPZ width at the current position of the equivalent elastic crack tip. The model is sketched in Fig. 1; axonometric view on single edge notched beam subjected to three-point bending (SEN-TPB) with the initial crack of length a_0, from where the effective crack (of current length a_i, the blue line) propagates during further loading. FPZ evolves around the crack tip; the envelope of FPZ's from all stages of fracture process from its beginning to its current point is indicated by the red line.

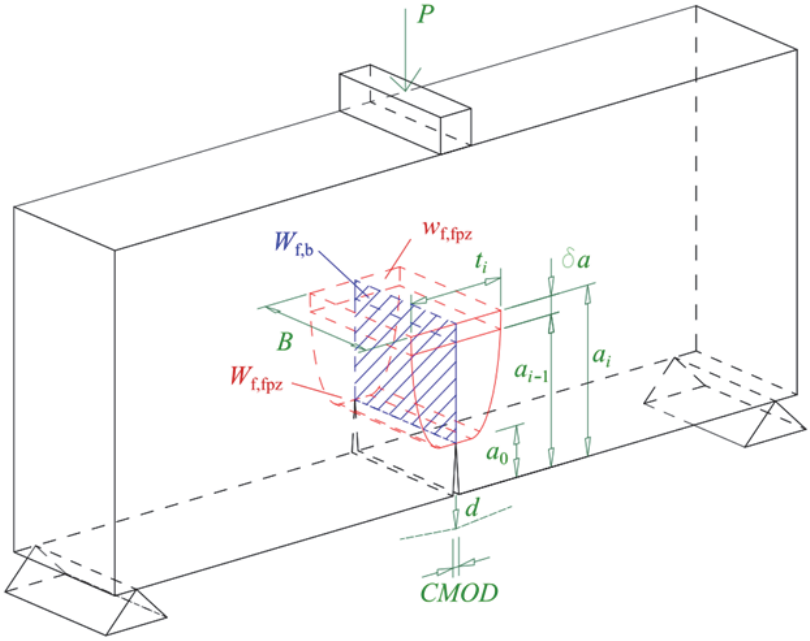

Figure 1: Sketch of the used model of the (effective) crack propagation and the cumulative FPZ extent advancement during the quasi-brittle fracture process in the SEN-TPB test specimen.

Construction of R-curves

As was noted above, the estimation of the $W_{f,b}$ and $W_{f,fpz}$ parts of the total amount of dissipated energy is performed from the recorded $P-d$ curves. The technique of separation of the whole area under the loading curve (interpreting the work of fracture W_f) into these two parts is following [23]. A specific load level is assigned to be the initial load by which the propagation of the effective crack begins (basically, in accordance with the double-K model [27,28]). The energy release rate G corresponding to this load is kept constant for the further effective crack propagation and designated as G_f. Thus, the area under the loading curve is divided into two regions by this curve corresponding to G_f: $W_{f,b}$ (under that curve) and $W_{f,fpz}$ (above it), see Fig. 2 left (the curve corresponding to the constant value of G_f is marked as "LEFM" there).
The practical implementation of this separation might be in many cases more convenient after a transformation of the analysed $P-d$ curve into the $R-a$ curve (or $R-\Delta a$, where Δa is the effective crack increment, or possibly $R-\alpha$, where $\alpha = a/W$ is the relative crack length). The equivalent elastic crack model [1] is employed for estimation of the current

(effective) crack length a at arbitrary stage of the fracture process. Determination of a is based on the difference between the initial compliance of the specimen with the crack of length a_0 and the specimen compliance at the current point of the $P-d$ diagram. Then, the value of fracture resistance R is calculated from the current load and effective crack length, most conveniently as

$$R = \frac{K_{Ic}^2}{E} = \frac{1}{E}\left(\sigma(P)\sqrt{a}\,Y(\alpha)\right)^2 \quad [\mathrm{J}] \tag{4}$$

where $\sigma(P)$ is the nominal stress in the line of the crack in the specimen due to the load P, $Y(\alpha)$ is the corresponding geometry function. Thus the value of $W_{f,b}$ is equal to the area under the G_f-a curve and $W_{f,fpz}$ to the area under the $R-a$ curve minus that under the G_f-a curve. Transformation of the $P-d$ diagram into the $R-\alpha$ curve with the indication of meanings of G_f and R, $W_{f,b}$, $W_{f,fpz}$ and W_f is shown in Fig. 2.

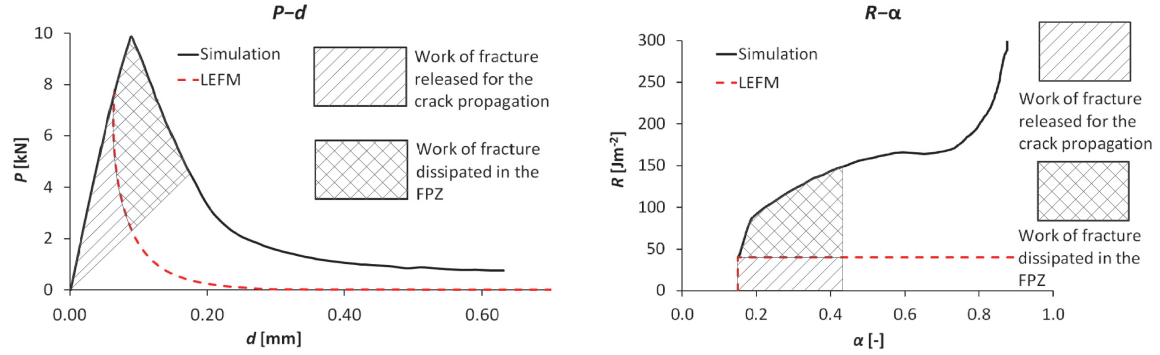

Figure 2: Indication of the individual portions of work of fracture at the current stage of fracture process in the loading diagram (left) and R-curve (right).

Estimation of process zone width.

Based on the constructed $R-a$ curve, the work of fracture dissipated in the FPZ, $W_{f,fpz}$, can be expressed from two monotonically increasing functions of the effective crack length a, i.e. W_f and $W_{f,b}$ (obtained by simple integration of the R-curve and G_f-curve for the quasi-brittle and the brittle fracture propagation, respectively), see Fig. 3 top left, as their subtraction, Fig. 3 top right.

After its differentiation with regard to a, the energy dissipated in the increment of the FPZ volume corresponding to effective crack increment equal to δa is obtained,

$$w_{f,fpz}(a) = \frac{\mathrm{d}W_{f,fpz}(a)}{\mathrm{d}a} \quad [\mathrm{Jm}^{-1}] \tag{5}$$

To facilitate the differentiation, the $W_{f,fpz}(a)$ function can be approximated by a polynomial function of a reasonable order (typically from 3rd to 6th, with a sufficient accuracy), see Fig. 3 top right. Under the above-mentioned assumptions, that the FPZ area increment is of the rectangular shape expressed as $\delta a \cdot t$ and the energy dissipation density H_f is uniform over the FPZ (i.e. also CDZ), the FPZ width can be expressed as

$$t(a) = \frac{w_{f,fpz}(a)}{BH_f} \quad [\mathrm{m}] \tag{6}$$

The procedure is illustrated in Fig. 3 top left, where the $W_f(a)$ and $W_{f,b}(a)$ curves are plotted, Fig. 3 top right, where the $W_{f,fpz}(a)$ curve is determined as the subtraction of $W_f(a)$ and $W_{f,b}(a)$, and Fig. 3 bottom, where the cumulative FPZ extent is plotted as the $t(a)$ function (displayed along the beam ligament).

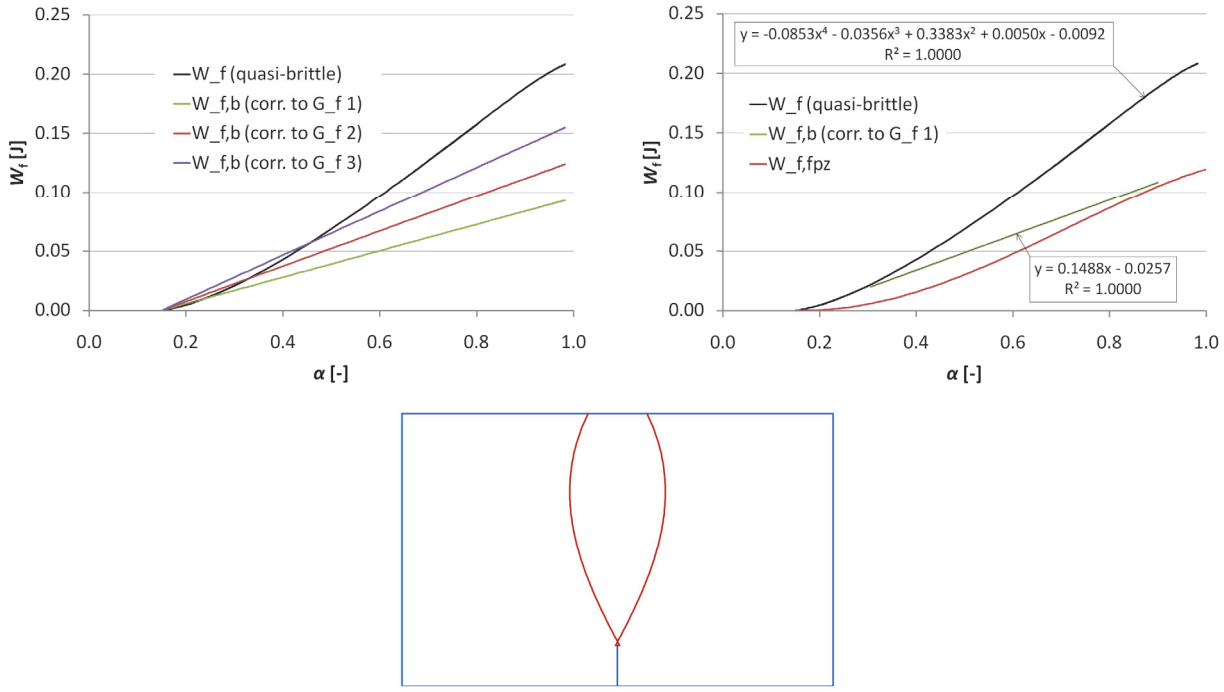

Figure 3: Plots of work of fracture due to quasi-brittle fracture $W_f(a)$ and brittle effective crack length propagation $W_{f,b}(a)$ (top left), their subtraction resulting in plot of cumulative energy dissipated in FPZ $W_{f,fpz}(a)$ (top right), and plot of FPZ envelope (bottom).

APPLICATION OF THE MODEL – EVALUATION OF EXPERIMENTAL DATA

Experiment by Hoover et al.

In the comprehensive experimental campaign reported in [24], four beam sizes of widths W = 500, 215, 93 and 40 mm (marked as A to D), with three relative notch lengths α_0 = 0.075, 0.15, and 0.3, were tested. Ratio of the smallest and the largest tested specimen is remarkable, namely 1:12.5. Several samples were tested for each W and α_0, for details see [24]. *P–d* diagrams were not measured properly in many cases; therefore, reconstructions of these diagrams based on the correctly recorded *P–CMOD* curves (*CMOD* stands for crack mouth opening displacement) were conducted with the help of numerical simulations in ATENA FEM programme [29] (parameters of the fracture-plastic material model used for concrete were identified according to the recorded *P−CMOD* diagrams) and subsequent data corrections were performed (details see in [30]). Nominal dimensions of the test specimen are shown in Tab. 1.

Specimen		Width W [mm]	Crack length a_0 [mm]	Rel. crack length $\alpha_0 = a_0/W$ [-]	Length L [mm]	Span S [mm]	Breadth B [mm]	Maximum FPZ width t_{max} [mm]
			3	0.075				42
D040	D	40	6	0.15	96	87.04	40	42
			12	0.3				58
			6.98	0.075				77
D093	C	93	13.95	0.15	223.2	209	40	74
			27.9	0.3				70
			16.13	0.075				122
D215	B	215	32.25	0.15	516	467.84	40	111
			64.5	0.3				143
			37.5	0.075				390
D500	A	500	75	0.15	1200	1088	40	350
			150	0.3				254

Table 1: Nominal dimensions of specimens from experiment [24]; estimated maximal widths of FPZ are shown in the right column.

Load–deflection diagrams for all beam depths and relative notch lengths in are shown Fig. 4. Recorded *P*–*d* curves (with some adjustments regarding the ascending part of the curve and unification of the elastic stiffness) are plotted by gray lines. Each diagram is complemented by a red line which corresponds to the FEM simulated response calibrated by recorded *P*−*CMOD* curve. In most of the cases, the simulated curve represents an average response of the individual specimen set very well. Each cell of the array of plots in Fig. 4 contains also a diagram with *R*–α curves corresponding to the *P*–*d* curves in the diagrams on the left.

These *R*-curves are shown also in Fig. 5 due to better understanding of their connection with the determined cumulative FPZ extents. Diagrams with the *R*-curves are plotted as α vs. *R*, where the axis of the relative crack length α is oriented along the specimen width *W*. In these graphs, a constant red curve is plotted, that corresponds to the specific energy released for propagation of the effective crack G_f. This value was estimated at 30 Jm^{-2} for all specimen sizes and notch lengths. This value was selected as the "optimum" from previously performed parametric study [30], where also other values of G_f were considered, see Fig. 3 left.

Plots of the determined FPZ extent envelopes within the beam of each size and notch depth present the main message shown in Fig. 5. The $t(a)$ functions (the curves corresponding to $W_{f,fpz}$) for each tested specimen are plotted in solid black line; grey lines represent parts of the function courses where too large error (due to measurement conducted to a limited value of *d* and its further extrapolations with polynomial functions and also due to increasing error of function of geometry with becoming close to the end of ligament used within the procedure of *R*-curve determination) was exhibited. The green line is the FPZ envelope corresponding to the FEM simulated "average" response.

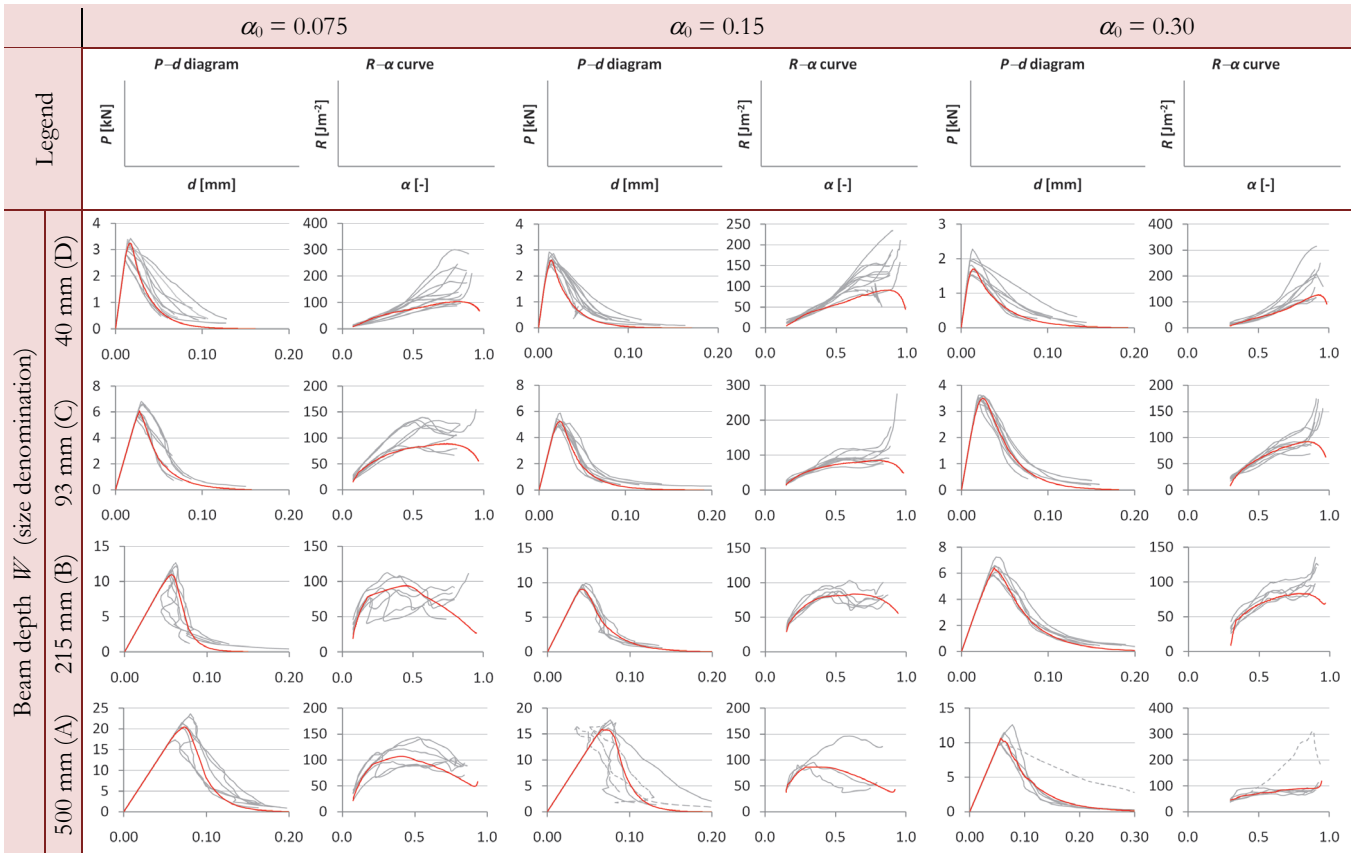

Figure 4: *P*–*d* diagrams and corresponding *R*–α curves for each specimen size *W* and relative notch length α_0; red curves correspond to simulated "average" response.

The value of the space density of energy dissipation in the FPZ was estimated at H_f = 215 Jm^{-3}. The ratio of the beam length and width is not displayed in real value in Fig. 5 due to better visual comparison FPZ extents in all beams.

The graph is complemented with blue dimension lines above each beam which indicate the mean values of estimated maximal FPZ widths (calculated from the black parts of the envelopes). These values are added to the right column of Tab. 1.

Experiment by Vidya Sagar & Raghu Prasad.

Extensive experimental study on fracture characteristics performed on notched beams of three sizes and notch lengths was published in [25,26]. Fracture tests on SEN-TPB specimens were accompanied also with acoustic emission (AE) scanning. Nominal dimensions of the tested specimens are shown in Tab. 2. Three specimens from each size and notch length configuration were tested, i.e. altogether 27 tested beams.

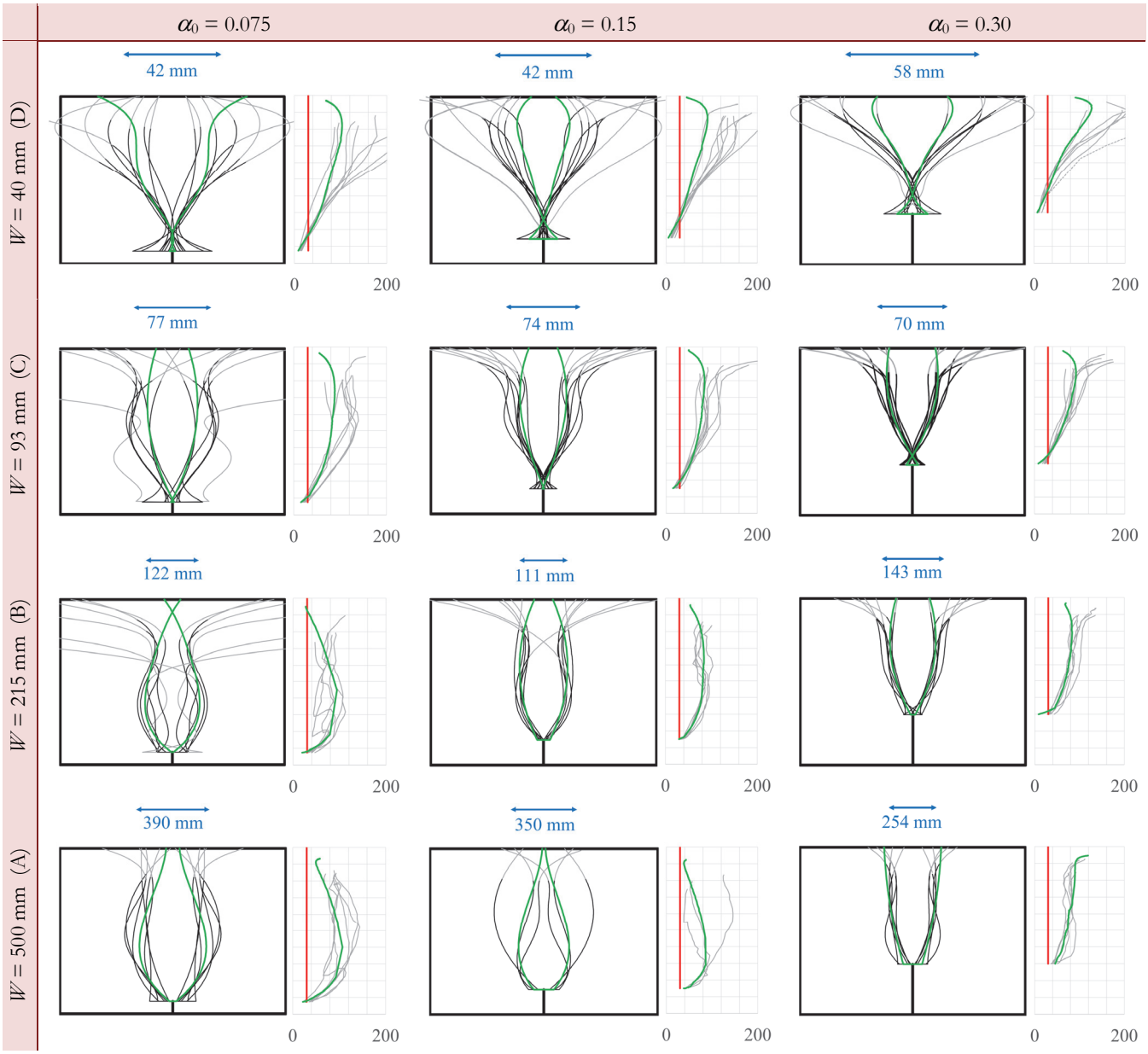

Figure 5: Scheme of the notched beam (the width W is scaled by a factor of 1.34 with respect to the length L; in reality $L/W = 2.4$) with the indication of the envelope of the FPZ for each tested sample and the FEM simulated response (green line); each figure is complemented with R-curve plots (grey lines, the red line corresponds to the G_f value released for the effective crack propagation).

These tests were conducted under the *CMOD* control, similarly as those in [24]. Again, the *P–d* diagrams were recorded simultaneously in order to evaluate fracture energy. However, no pure deflection of the beam was recorded but a quantity including also crushing and plastic deformation at supports, deformation of the loading machine frame etc., i.e. evaluation of the recorded *P–d* diagrams was not appropriate. Therefore, the ATENA FEM code [29] was utilized to simulate the fracture test according to the correctly recorded *P–CMOD* curves, similarly as in the previous experimental campaign.

Again, a simple trial and error optimization technique was performed for identification of the fracture-plastic (cohesive crack-based) material model in the employed code, details can be found in [31].

Reconstructed *P*–*d* curves (via numerical simulations) with corresponding *R*–α curves for all beam depths and relative notch lengths are shown in Fig. 6. It can be seen that in this case, contrary to the previous experimental set, the tails of the *R*-curves grow up, which is most likely caused by the accumulated numerical error in the area of tails of the simulated *P*–*d* diagrams. Therefore, estimates of the *R*-curve ends (horizontal lines) are used for further analysis of the FPZ extent. They are depicted in the *R*-curve plots by dotted lines (for relative crack lengths α_0 = 0.15 and 0.3) in Fig. 7.

Specimen		Width W [mm]	Crack length a_0 [mm]	Rel. crack length $\alpha_0 = a_0/W$ [-]	Length L [mm]	Span S [mm]	Breadth B [mm]
Small	S	80	12	0.15	290	240	80
			24	0.3			
			40	0.5			
Medium	M	160	24	0.15	530	480	80
			48	0.3			
			80	0.5			
Large	L	320	48	0.15	1010	960	80
			96	0.3			
			160	0.5			

Table 2: Nominal dimensions of specimens from the experiment [25].

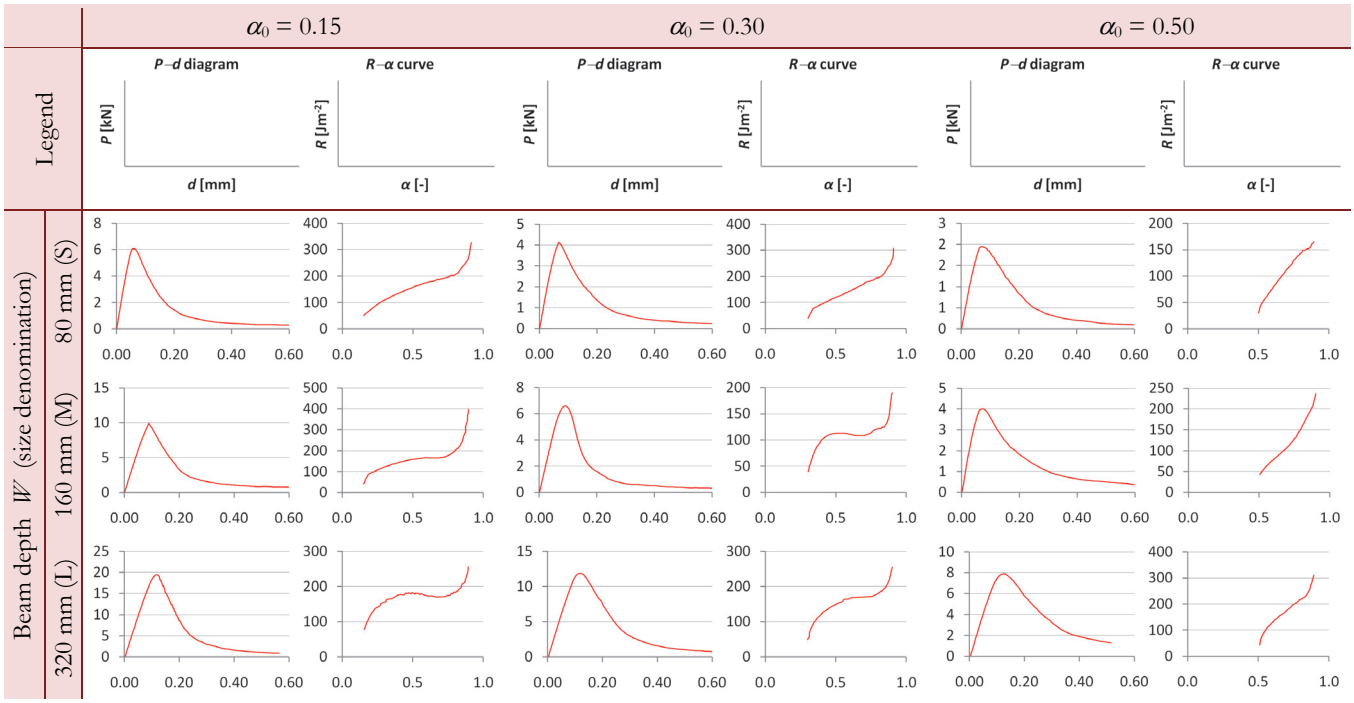

Figure 6: Simulated *P*–*d* diagrams and corresponding *R*–α curves for each specimen size W and relative notch length α_0 set.

The envelopes of FPZ extents corresponding to these beams are displayed in Fig. 7. In this case, they are plotted in three graphs for the small, middle and large beams, respectively. All three notch lengths for each beam size are included in one diagram. The diverging branches of the FPZ envelopes are displayed in gray, those corresponding to the constant *R* estimates are displayed as dotted lines in the colours matching the related *R*-curve. The two parameters of this tested

model, i.e. the specific energy for the effective crack propagation G_f and the space density of energy dissipation in FPZ H_f, were estimated at values 40 Jm^{-2} and 215 Jm^{-3}, respectively, for the experiment [25].

DISCUSSION OF RESULTS

Experiment by Hoover et al.

The compliance-based constructed *R*-curves from experiment [24] exhibit rather different trends for the small and large beams. Small samples (mainly D, also C with the longest notches) are characteristic by increasing trend of *R* along the specimen ligament, which is even more pronounced close to its end. A steady progress of *R* is observed for large samples (A and B) with eventually decreasing trend near the end of the ligament (mainly for the shortest notches).

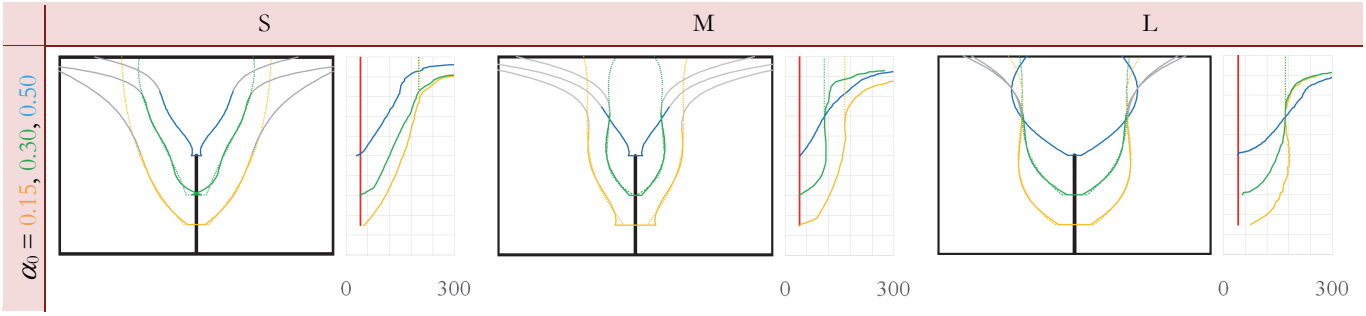

Figure 7: Scheme of the notched beam (the width W is scaled by a factor of 2.42 with respect to the length L; in reality S/W = 3.3) with the indication of the envelope of the FPZ for the FEM simulated response for each relative crack length; each figure is complemented with *R*-curve plots (the red line corresponds to the G_f value released for the effective crack propagation).

The FPZ extent seems to be described by the constructed envelope curves reasonably well except the very beginning and the end of the ligament. The FPZ extent estimation is corrupted at the ligament ends in the cases where significant increases in the *R*-curve trends are observed. This increase in *R* in that area is caused by an error of measurement/modelling accumulated at the ends of descending branches of the recorded/simulated loading curves. The odd shape of the FPZ envelope at the beginning of the fracture propagation from the notch (the "fish tail" shape) that is observed mainly for small sizes (D, also C and B for the longest notches) corresponds actually to negative value of $W_{f,fpz}$ at these points. This is caused by too high value of G_f at these stages of fracture. This feature could be eliminated using non-constant value of G_f (modelled e.g. by some increasing function with a plateau), which was undesirable in this study. Both parameters of the models were considered as constants.

Based on Fig. 5, it can be concluded that the introduced simple model captures the size/geometry effect on the fracture parameters reasonably well. The size of FPZ for smaller specimens takes a relatively larger part of the total volume of the specimen than it occurs in the case of larger specimens. The large beams exhibit much more brittle behaviour; therefore, the energy released for effective crack propagation $W_{f,b}$ occupies a larger portion of the whole energy W_f released during fracture.

Maximum widths of the FPZ t_{max} shown in Tab. 1 are plotted for the individual notch lengths as functions of the beam size in Fig. 8 left. The increasing trend is obvious. After relating t_{max} to the specimen size, all the data were fitted. Based on the fact that for an infinitely large specimen the ratio t_{max}/W must tend to zero, a power function was chosen. The regression is plotted in Fig. 8 right in the bi-logarithmic scale.

As is evident from Eq. 6, the FPZ width is inversely proportional to the space density of energy dissipation in FPZ H_f. Thus, the t_{max} value is dependent on the H_f value considered in the study. The authors must admit, that the value was guessed in this case. However, its much proper estimation can be possibly performed based on experimental observations of FPZ using e.g. AE scanning (see below) or/and radiography [32–34]. Alternatively, analytical estimation of the FPZ extent based on matching the crack-tip stress state description and strength properties of the material (via proper failure criteria) might be also helpful for this task, see e.g. [16,17,35–37]. Nevertheless, the power law proposed for the FPZ width estimation would apply also for different values of H_f as the value of t_{max} would be scaled by the same factor for all sizes.

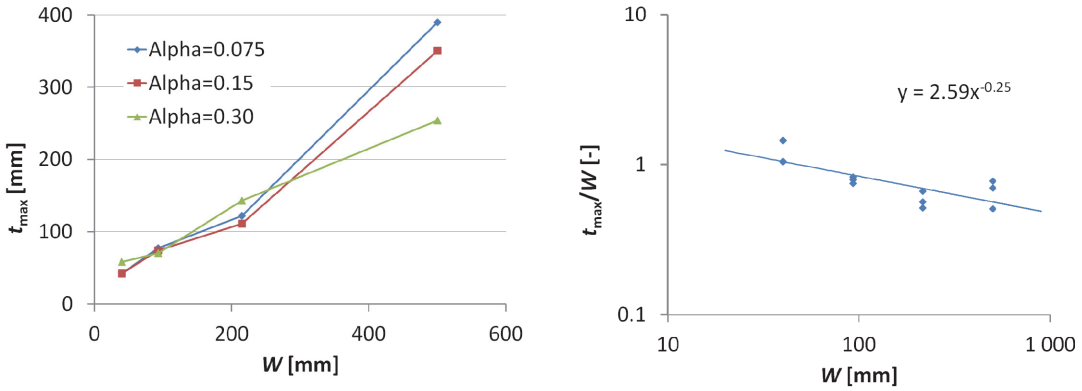

Figure 8: Maximum width of the FPZ extent envelope for all specimen sizes: Dependencies plotted individually for each notch length (left), regression of all the data by power function.

Experiment by Vidya Sagar & Raghu Prasad.

The range of specimen sizes tested in this campaign was considerably smaller than that in [24]; however, extents of cumulative FPZ estimated from localized AE events were reported. Fig. 9 shows displays of AE events locations at the end of the fracture test. Unfortunately, only very limited amount of these results from the whole campaign is available in the published papers [25,26]. Thus, the comparison of the cumulative FPZ extents from AE measurement with that of the proposed model is limited here only to the cases with the shortest notches. Similarly to Fig. 7, the diverging parts of the FPZ envelopes are in gray and the estimates of these parts based on the constant R in this portion of the specimen ligament are displayed by the red dotted line. A relatively good agreement was obtained.

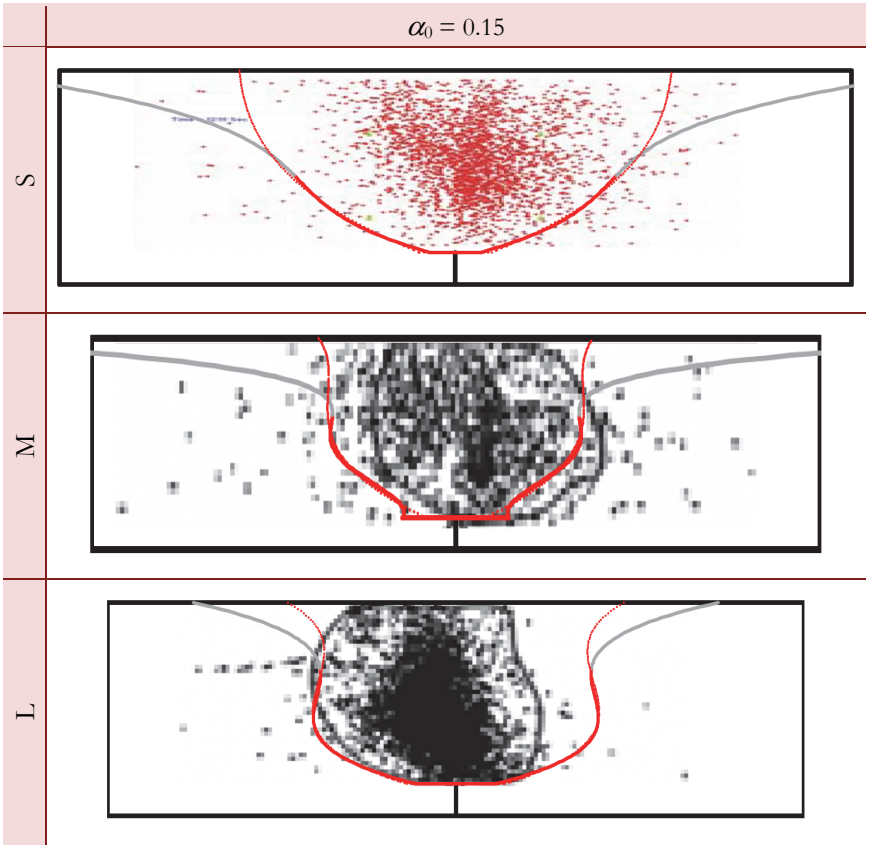

Figure 9: Notched beams of all tested sizes with the shortest relative notch length with the indication of the envelope of the FPZ for the FEM simulated response compared to localized AE events (top figure adopted from [26], middle and bottom from [25]).

CONCLUSIONS

The paper presents a new simple model based on two parameters which has an ambition to describe the quasi-brittle fracture in a way that does not depend on the specimen size, shape and boundary conditions. This approach models the nonlinear fracture process via a separation of the dissipated energy into the amount released for the propagation of the effective crack and the amount dissipated in the volume of FPZ. Parameters of this rather simplified model of quasi-brittle crack growth, namely the resistance to the effective crack propagation (or the fracture energy) G_f and the density of energy dissipation in the FPZ H_f, are determined based on records of the fracture tests, i.e. from the recorded loading curves, and are regarded as material properties.

The model is (partially) validated here by data from experimental campaigns published in the literature, concerning SEN-TPB tests on specimens of different sizes and relative notch lengths. The model parameters were determined in a more or less heuristic way in this study. Thus, a closer connection with methods of evaluation of the FPZ extent using direct experimental imaging techniques (AE, X-ray and similar) is necessary. Own experimental works in this regard are ongoing/in preparation at present. Alternatively, indirect analytical stress-based methods can be applied, which must be connected to test results on material strength. Application of soft-computing optimization methods for this task is also considered for future studies.

ACKNOWLEDGEMENT

Financial support from the Czech Science Foundation (project No. 15-07210S) and Brno University of Technology, Specific Research programme (project No. FAST-S-16-3475) is gratefully acknowledged.

REFERENCES

[1] Karihaloo, B.L., Fracture mechanics and structural concrete, Longman Sci. & Techn., New York (1995).
[2] Bažant, Z.P., Planas, J., Fracture and size effect of concrete and other quasi-brittle materials, CRC Press, Boca Raton (1998).
[3] Shah, S.P., Swartz, S.E., Ouyang, C., Fracture Mechanics of Concrete: Applications of Fracture Mechanics to Concrete, Rock and Other Quasi-Brittle Materials, Wiley (1995).
[4] van Mier, J.G.M., Fracture processes of concrete, CRC Press (1997).
[5] Bažant, Z.P., Kazemi, M.T., Size dependence of concrete fracture energy determined by RILEM work-of-fracture method, Int. J. Fract., 51(2) (1991) 121–138.
[6] Elices, M., Guinea, G. V., Planas, J., Measurement of the fracture energy using three-point bend tests: part 3–Influence of cutting the P–δ tail, Mater. Struct., 25(6) (1992) 327–334.
[7] Hu, X.-Z., Wittmann, F.H., Size effect on toughness induced by crack close to free surface. Engng. Fract. Mech., 65 (2000) 209–221.
[8] Trunk, B., Wittmann, F.H., Influence of size on fracture energy of concrete, Mater. Struct, 36 (2001) 260–265.
[9] Karihaloo, B.L., Abdalla, H.M., Imjai, T., A simple method for determining the true fracture energy of concrete. Mag. Concr. Res., 55 (2003) 471–481.
[10] Duan, K., Hu, X.-Z., Wittmann, F.H., Boundary effect on concrete fracture and non-constant fracture energy distribution, Engng. Fract. Mech., 70 (2003) 2257–2268.
[11] Bažant, Z.P., Yu, Q., Size effect in fracture of concrete specimens and structures: new problems and progress, in Li V.C. et al. (eds.), Proc. of the 5th international conference on fracture mechanics of concrete and concrete structures, Vail Colorado, USA, 12–16 April, 2004, 153–162.
[12] Hu, X.-Z., Duan, K., Size effect: Influence of proximity of fracture process zone to specimen boundary, Engng. Fract. Mech., 74 (2007) 1093–1100.
[13] Yu, Q., Le, J., Hoover, C., Bažant, Z., Problems with Hu-Duan Boundary Effect Model and its comparison to Size-Shape Effect Law for quasi-brittle fracture, J. Eng. Mech., 89 (2010) 40–50. DOI: 10.1061/(ASCE)EM.1943-7889.
[14] Cifuentes, H., Alcalde, M., Medina, F., Measuring the size-independent fracture energy of concrete, Strain, 49(1) (2013) 54–59. DOI: 10.1111/str.12012.

[15] RILEM Committee FMT 50, Determination of the fracture energy of mortar and concrete by means of three-point bend tests on notched beams, Mater. Structures, 18 (1985) 285–296.
[16] Veselý, V., Frantík, P., Reconstruction of fracture process zone during tensile failure of quasi- brittle materials, Appl. Comp. Mech., 4(2) (2010) 237–250.
[17] Veselý, V., Frantík, P., An application for the fracture characterisation of quasi- brittle materials taking into account fracture process zone influence, Adv. Eng. Softw., 72 (2014) 66–76. DOI: 10.1016/j.advengsoft.2013.06.004.
[18] Frantík, P., Veselý, V., Keršner, Z., Parallelization of lattice modelling for estimation of fracture process zone extent in cementitious composites, Adv. Eng. Softw., 60–61 (2013) 48–57. DOI: 10.1016/j.advengsoft.2012.11.020.
[19] Hillerborg, A., Modéer, M., Petersson, P-E., Analysis of crack formation and crack growth in concrete by means of fracture mechanics and finite elements, Cem. Concr. Res., 6 (1976) 773–782.
[20] Bažant, Z.P., Oh, B.-H., Crack band theory for fracture of concrete, Mater. Struct., 16 (1983) 155–177.
[21] Veselý, V., Frantík, P., Keršner, Z. Cracked volume specified work of fracture, in: Topping, B.H-V., Costa Neves, L.F., Barros, R.C. (eds), Proceedings of the 12th int. conf on civil, structural and environmental engineering computing. Stirlingshire: Civil-Comp Press (2009).
[22] Veselý, V., Frantík, P., Vidya Sagar, R., Štafa, M., Pail, T., Balanced energy dissipation at propagating crack tip in quasi-brittle materials? – Analysis via soft-computing methods, Key Eng. Mat., 577–578 (2014) 269–272. DOI: 10.4028/www.scientific.net/KEM.577-578.269.
[23] Klon, J., Veselý, V., Energy dissipation during quasi-brittle fracture associated with the crack and the fracture process zone progression, Key Eng. Mat., 665 (2016) 261–264. DOI:10.4028/www.scienti_c.net/KEM.665.261.
[24] Hoover, Ch.G., Bažant, Z.P., Vorel, J., Wendner, R., Hubler, M.H., Comprehensive concrete fracture tests: Description and results, Engng. Fract. Mech., 114 (2013) 92–103.
[25] Vidya Sagar, R., Raghu Prasad, B.K., An experimental study on fracture process zone in HSC three point bend beam specimen using acoustic emission method, Journal of Structural Engineering, 36(1) (2009) 397–407.
[26] Vidya Sagar, R., Raghu Prasad, B.K., Fracture analysis of concrete using singular fractal functions with lattice beam network and confirmation with acoustic emission study, Theoretical and Applied Fracture Mechanics, 55 (2011) 192–205. DOI:10.1016/j.tafmec.2011.07.003.
[27] Xu, S., Reinhardt, H.W., Crack extension resistance and fracture properties of quasi-brittle softening materials like concrete based on the complete process of fracture, International Journal of Fracture, 92 (1998) 71–99.
[28] Reinhardt, H.W., Xu, S., Crack extension resistance based on the cohesive force in concrete, Engng. Fract. Mech., 64 (1999) 563–587.
[29] Červenka, V., Jendele, L., Červenka, J., ATENA Program Documentation, Cervenka Consulting, Prague (2010).
[30] Klon, J., Modeling of fracture process in quasi-brittle materials, Master's Thesis, Brno University of Technology, Faculty of Civil Engineering, Institute of Structural Mechanics, Brno (2016).
[31] Klon, J. Fracture process zone and energy dissipation during fracture of quasi-brittle materials, Bachelor's Thesis, Brno University of Technology, Faculty of Civil Engineering, Institute of Structural Mechanics, Brno (2014).
[32] Otsuka, K., Date, H., Fracture process zone in concrete tension specimen, Engineering Fracture Mechanics, 65 (2000) 111–131.
[33] Kumpová, I., Fíla, T., Vavřík, D., Keršner, Z. X-ray dynamic observation of the evolution of the fracture process zone in a quasi-brittle specimen, Journal of Instrumentation, 10 (2015). DOI:10.1088/1748-0221/10/08/C08004.
[34] Vavřík, D., Jandejsek, I., Fíla, T., Veselý, V., Radiographic observation and semi-analytical reconstruction of fracture process zone in silicate composite specimen, Acta Technica, 58 (2013) 315–326.
[35] Veselý, V., Sobek, J., Tesař, D., Frantík, P., Pail, T., Seitl, S., Multi-parameter approximation of stress field in a cracked specimen using purpose-built Java applications, Frattura ed Integrità Strutturale, 33 (2015) 120–133.
[36] Veselý, V., Sobek, J., Malíková, L., Frantík, P., Seitl, S., Multi-parameter crack tip stress state description for estimation of fracture process zone extent in silicate composite WST specimens, Frattura ed Integrità Strutturale, 25 (2013) 69–78.
[37] Malíková, L., Veselý, V. The influence of higher-order terms of Williams series on a more accurate description of stress fields around the crack tip. Fatigue & Fracture of Engineering Materials & Structures, 38 (2015) 91–103.